Modeling reactive ammonia uptake by secondary organic aerosol in CMAQ: application to continental US

Shupeng Zhu[1], Jeremy R. Horne[1], Julia Montoya-Aguilera[2], Mallory L. Hinks[2], Sergey A. Nizkorodov[2], and Donald Dabdub[1]

[1]Computational Environmental Sciences Laboratory, Department of Mechanical & Aerospace Engineering, University of California, Irvine, Irvine, CA, 92697-3975, USA
[2]Department of Chemistry, University of California, Irvine, Irvine, CA, 92697-3975, USA

Correspondence to: Donald Dabdub (ddabdub@uci.edu)

Abstract. Ammonium salts such as ammonium nitrate and ammonium sulfate constitute an important fraction of the total fine particulate matter ($PM_{2.5}$) mass. While the conversion of inorganic gases into particulate phase sulfate, nitrate, and ammonium is now well understood, there is considerable uncertainty over interactions between gas-phase ammonia and secondary organic aerosols (SOA). Observations have confirmed that ammonia can react with carbonyl compounds in SOA, forming nitrogen-containing organic compounds (NOC). This chemistry consumes gas-phase NH_3 and may therefore affect the amount of ammonium nitrate and ammonium sulfate in particulate matter (PM) as well as particle acidity. In order to investigate the importance of such reactions, a first-order loss rate for ammonia onto SOA was implemented into the Community Multiscale Air Quality (CMAQ) model based on the ammonia uptake coefficients reported in the literature. Simulations over the continental US were performed for the winter and summer of 2011 with a range of uptake coefficients (10^{-3} - 10^{-5}). Simulation results indicate that a significant reduction in gas-phase ammonia may be possible due to its uptake onto SOA; domain-averaged ammonia concentrations decrease by 31.3 % in the winter, and 67.0 % in the summer with the highest uptake coefficient (10^{-3}). As a result, the concentration of particulate matter is also significantly affected, with a distinct spatial pattern over different seasons. PM concentrations decreased during the winter, largely due to the reduction in ammonium nitrate concentrations. On the other hand, PM concentrations increased during the summer due to increased biogenic SOA production resulting from enhanced acid-catalyzed uptake of isoprene-derived epoxides. Since ammonia emissions are expected to increase in the future, it is important to include NH_3 + SOA chemistry in air quality models.

1 Introduction

As the most abundant basic gas in the atmosphere (Behera et al., 2013), gaseous ammonia (NH_3) has long been considered responsible for controlling the eutrophication and acidification of ecosystems (Sutton et al., 1993; Erisman et al., 2008; Sheppard et al., 2011). More recently, studies also demonstrated the importance of ammonia in the formation of airborne fine particulate matter ($PM_{2.5}$) (West et al., 1999; Vayenas et al., 2005; Wang et al., 2013). Through reactions with acidic species, ammonia is converted into ammonium salts, such as ammonium nitrate and ammonium sulfate, which constitute an important fraction of total $PM_{2.5}$ mass (Behera and Sharma, 2010). These aerosols have been proven to affect human health (Pope III et al., 2002; Lelieveld et al., 2015), visibility (Ye et al., 2011) and the atmospheric radiative balance (Xu and Penner, 2012; Park et al., 2014). In the US, the largest ammonia emission source is agricultural activity (85% of total US ammonia emissions) (Pinder et al., 2004, 2006), largely from animal waste and commercial fertilizer application, such as the intensive farming in California's central valley (Jovan and McCune, 2005) and industrialized hog farms in central North Carolina (McCulloch et al., 1998; Aneja et al., 2000). The ammonia rich plumes from those areas drive most of the nitric acid into the particle phase, resulting in high $PM_{2.5}$ concentrations in those regions (Neuman et al., 2003; Baek and Aneja, 2004). Recent studies have also shown that atmospheric ammonia has increased during the last two decades, a trend that is expected to continue as a result of global warming, increasing agricultural activity and intensifying fertilizer use due to growing population (Galloway et al., 2008; Amann et al., 2013; Warner et al., 2017).

While the conversion of inorganic gases into particulate phase sulfate, nitrate, and ammonium is now fairly well understood (Seinfeld and Pandis, 2016), there is considerable uncertainty over interactions between gas phase ammonia and organic compounds in secondary organic aerosols (SOA). Laboratory studies have shown that ammonia can react with SOA compounds in two ways. It can either react with organic acids to form ammonium salts (Na et al., 2007), or participate in reactions with certain carbonyl compounds forming heterocyclic nitrogen-containing organic compounds (NOC) (Updyke et al., 2012; Laskin et al., 2015). In addition, a browning effect on SOA under NH_3 exposure is observed by Updyke et al. (2012), indicating the production of light-absorbing products. These processes are not included in current air quality models, which could lead to over estimation of gaseous ammonia concentrations, and thus inorganic aerosol concentration. Additionally, the neglect of these two processes may also result in under estimation of organics aerosol, especially species related to acid catalyzed reactions (Lin et al., 2013) and in incorrect prediction of aerosol particle acidity.

Recently, chemical uptake coefficients for ammonia onto SOA were reported for the first time by Liu et al. (2015). Those coefficients were on the order of $\sim 10^{-3}$-10^{-2} for fresh SOA, decreasing significantly to $< 10^{-5}$ after 6h of reaction. They observed that the NOC mass contributed 8.9 ± 1.7 and 31.5 ± 4.4 wt% to the total α-pinene and m-xylene-derived SOA, respectively, and 4-15 wt% of the total nitrogen in the system. If such large fraction of SOA compounds can be converted to NOC it can have large effect on both NH_3 and PM concentrations.

In this work, we investigate the impact of ammonia uptake by SOA on $PM_{2.5}$ and NH_3 concentrations, by implementing a first-order loss rate for ammonia onto SOA into the Community Multiscale Air Quality (CMAQ) modeling system based on ammonia uptake coefficients reported by Liu et al. (2015). Air quality simulations over the continental US were performed with a range of uptake coefficients to determine the sensitivity of $PM_{2.5}$ and NH_3 concentration to the magnitude of the uptake coefficient. Furthermore, in order to investigate the seasonal impact on this process, simulations were conducted for both winter and summer. The modeling method used in this analysis will first be presented in section 2. Then, simulation results will be analyzed based on both observational data and sensitivity comparisons between different scenarios in section 3. Finally, in section 4, the importance of including this process in air quality models will be discussed.

2 Methodology

The CMAQ modeling system (Byun and Schere, 2006) is a widely used state-of-the-art chemical transport model. In the United States, it is among the most commonly used air quality models in attainment demonstrations for National Ambient Air Quality Standards for ozone and $PM_{2.5}$ (USEPA, 2007). In this study, eight simulations were conducted using the latest 2017 release of CMAQ (Version 5.2), including one base case simulation for the winter (Jan. 1 - Feb. 27, 2011), one base case simulation for the summer (Jul. 1 - Aug. 30, 2011), and three different NH_3 uptake scenarios for each period. The Carbon Bond version 6 (CB6) mechanism (Yarwood et al., 2010) was used for the gas-phase chemistry, which includes 127 species as detailed on the website (Adams, 2017), and the AERO6 module was used for aerosol dynamics, which includes 21 inorganic species and 34 organic species (28 SOA and 6 primary organic species) as detailed on the CMASWIKI website (Pye, 2016). The modeling domain used in this study covers the contiguous US using a 12 km × 12 km horizontal grid resolution (resulting in 396 (x) × 246 (y) = 97,416 grid cells) and a 29-layer logarithmic vertical structure (set on a terrain following sigma coordinate, from the surface to 50 hPa) with the depth of the first layer around 26 m. Only the simulation results from the first layer, representative of ground level, were used for the analysis in this study.

The meteorological fields were derived from NCEP FNL (Final) Operational Global Analysis data (NCEP, 2000) using the Weather Research and Forecasting Model (WRF, version 3.7) (Skamarock et al., 2008), with the MODIS land use database (Friedl et al., 2010) and the YSU parametrization (Hong et al., 2006) for the planetary boundary layer. The WSM3 scheme (Hong et al., 2004) was used for the microphysics option of WRF, and the Kain - Fritsch convective parametrization (Kain, 2004) was used for cumulus physics. These fields were then processed using Version 4.3 of Meteorology Chemistry Interface Program (MCIP) (Otte and Pleim, 2010). The initial and boundary conditions were obtained from the Model for OZone And Related chemical Tracers (Mozart v2.0) (Horowitz et al., 2003). Emissions were generated based on the 2014 National Emissions Inventory (NEI) (EPA, 2017a) and processed by the Sparse Matrix Operator Kernel Emission (SMOKE, version 4.5) processor (EPA, 2017b). Biogenic emissions were obtained from the Biogenic Emission Inventory System (BEIS) (Pierce and Waldruff, 1991), and emissions from cars, trucks, and motorcycles were calculated with MOBILE6 (EPA, 2003).

In this study, the AERO6 module in CMAQ was updated to simulate the heterogeneous uptake of NH_3 by SOA. AERO6 used the modal representation to simulate aerosol dynamics (Binkowski and Roselle, 2003). The size distribution of the aerosol particles is represented by 3 log-normal modes: the Aitken mode (size up to approximately 0.1 μm), the accumulation mode (size between 0.1 μm to 2.5 μm) and the coarse mode (size between 2.5 μm to 10 μm). The particles are assumed to be internally mixed within each mode. In the AERO6 modal approach, three integral properties of the size distribution are followed for mode j: the total particle number concentration N_j, the total wet surface area concentration S_j, and the total mass concentration m_{ij} of each individual chemical component i. In order to calculate the total uptake of NH_3 by SOA, one must know the representative wet surface area concentration of SOA (S_{SOA}) (SOA hygroscopic growth is not considered in the model), that can be calculated as follows (assuming a uniform density across different chemical components):

$$S_{SOA} = \sum_{j=1}^{x}(S_j \times \frac{\sum_{i=1}^{y} m_{ij}}{\sum_{k=1}^{z} m_{kj}}) \tag{1}$$

where y is the total number of SOA species in mode j, z is the total number of aerosol species in mode j, and x is the total number of modes that contain SOA species. Here, x=2 since SOA only exist in the Atiken mode and the accumulation mode. From S_{SOA} the first order rate of NH_3 uptake can be calculated as:

$$k = \gamma \times \frac{v_{NH_3} \times S_{SOA}}{4} \tag{2}$$

where γ is the reactive uptake coefficient for ammonia, and v_{NH_3} is the average speed of NH_3 molecules (609 m/s at 298 K). The above calculations were performed separately for each grid cell at every time step to obtain the effective first-order rate constant for each individual cell at each time step. The first-order rate constant of NH_3 uptake was then multiplied by the gas-phase NH_3 concentration to determine the loss rate of NH_3 in each cell at each time step.

In this study, all NH_3 taken up by SOA carbonyls is assumed to form NOCs, such as secondary imines and heteroaromatic compounds (Laskin et al., 2015). In this reaction, the carbonyl group of an SOA compounds is converted into an imine group and a molecule of water is produced as a by-product. The imine product can further react by an intermolecular cyclization to produce heterocyclic organic compounds, with a loss of an additional water molecule (Laskin et al., 2014). The difference in molecular weights of two H_2O molecules and one NH_3 molecule (2 ×18 - 17 = 19 g/mol) is small relative to a molecular weight of a typical SOA compounds (about 200 g/mol). Therefore, for the sake of simplicity, we neglected the loss of the mass of particulate organics mass directly due to the NH_3 uptake in this simulation. This assumption is supported by experimental observations described by Horne et al. (2018), in which SOA particles exposed to ammonia in a smog chamber did not change their size distribution but showed clear evidence of incorporation of organic nitrogen into the particles in on-line and off-line mass spectra. Although, the NH_3 uptake process does not directly impact the mass of SOA, it can affect the SOA mass indirectly as particle acidity is altered due to this process, which will be discussed in section 3.2.3. Figure S1 in the SI section shows a schematic representation of the NH_3 reactions considered in the model, including reversible function of inorganic salts and irreversible formation of NOC. The ability of NOCs to neutralize inorganic acids to form salts is not considered (see Figure S1.) because NOCs are generally much weaker bases (e.g., imine $pK_b \sim 10$, pyrrole pK_b = 13.6, pK_b = 8.8) compared to NH_3 (pK_b = 4.8). In other words, once NH_3 is converted into NOC, it is no longer available to make inorganic salts of nitrate and sulfate.

As current laboratory data are not detailed enough to model the chemical uptake coefficient of ammonia by individual SOA species explicitly, a range of uptake coefficients was selected and applied to all SOA species. In the future, this approach can be refined by adopting more explicit reactions between ammonia and various types of SOA compounds. The ammonia uptake coefficients (γ) used in this study were based on the values reported in the work of Liu et al. (2015), as well as the maximum possible extended conversion of SOA carbonyls into NOC. Liu et al. (2015) reported a range of possible uptake coefficients from 10^{-5} to 10^{-2}. However, some of our initial modeling tests showed that the use of 10^{-2} uptake coefficient value would lead to an unrealistic amount of NH_3 taken up by SOA, where within a single time step, the number of moles of NH_3 taken up exceeded 10% of the total moles of SOA in one grid cell. Experiments (Liu et al., 2015; Horne et al., 2018) suggest that only 10% or less of SOA molecules can react with NH_3 to form nitrogen-containing organic compounds (NOC). Additionally, in the study of Liu et al. (2015), the uptake coefficients are measured based on only a few SOA species (SOA formed from ozonolysis of α-pinene and OH oxidation of m-xylene); other SOA species might not have the same reactivity. Furthermore, the highest value of uptake coefficient was only observed at the initial period of the experiment of Liu et al. (2015) and decreased rapidly over time. Based on the considerations above, uptake coefficient of 10^{-3} was considered a more reasonable upper limit value for our application instead of 10^{-2}. Thus, four simulations were performed for each period to investigate the sensitivity of NH_3 removal to changes in the uptake coefficient: (a) base case with no NH_3 uptake, (b) NH_3 uptake with $\gamma = 10^{-3}$, (c) NH_3 uptake with $\gamma = 10^{-4}$, (d) NH_3 uptake with $\gamma = 10^{-5}$.

Results from each simulation were evaluated by comparing with observations from multiple monitoring networks. Then simulation results for scenario (b), (c) and (d) are compared to the base case results in (a) to determine the impact of different uptake coefficients on different gas and particle phase species. The value of γ was assumed to remain constant in each scenario (i.e., no saturation or aging effects), which means each scenario represents an upper limit for the amount of NH_3 that would be taken up by SOA with the chosen value of the uptake coefficient. No further changes were made to the model or its inputs between each scenario. Results of the first 7 days of each simulations were discarded as a model spin up period to minimize the effect of initial conditions and allow sufficient time for NH_3 removal process to occur.

3 Results and Discussion

3.1 Model validation

First, base case simulation results of $PM_{2.5}$, PM_{10} and O_3 are compared with the observations from the U.S. Environmental Protection Agency's Air Quality System (AQS) to evaluate the model performance. The AQS network (https://www.epa.gov/aqs) is geographically diverse and spans the entire US. It is also an excellent source of quality assured measurements, with hourly recorded concentrations for $PM_{2.5}$, PM_{10} and O_3. The definitions of the statistical parameters used in this study are detailed in the supporting information (SI) (Table S1).

Table 1 shows good model performance for O_3, as the statistics meet the recommended performance criteria ($|\mathrm{MNGB}| \leq 15\%$ and MNGE $\leq 30\%$) (Russell and Dennis, 2000). Additionally, the maps of MNGB values of O_3 measured by individual stations are available in the SI section (Figure S2). This maps show that most of the stations have low bias with some underestimation over the north-east in the winter and some general overestimation around the country in the summer. Only the two base cases simulations are shown in Table 1 and Figure S2, because the change in NH_3 uptake coefficient has no impact on O_3 in the model. Table 2 shows the statistics for $PM_{2.5}$ for both the summer and winter. Cases satisfied the model performance criteria proposed by (Boylan and Russell, 2006) with MFE $\leq$ 75% and $|\mathrm{MFB}| \leq 60\%$. Additionally, the maps of MFB values of $PM_{2.5}$ measured by individual stations are available in the SI section (Figure S3). The model performance for winter is much better than for the summer, as the amount of $PM_{2.5}$ is overestimated during the summer. The impact of different NH_3 uptake coefficients on $PM_{2.5}$ is also reflected in the statistics. For the winter, increasing the NH_3 uptake coefficient leads to a decrease of the total $PM_{2.5}$ and a slightly better model performance when compared to the observations. On the contrary, larger NH_3 uptake coefficients cause higher $PM_{2.5}$ concentration during the summer, resulting in a larger discrepancies compared with measurements. The reasons for such seasonal differences will be analyzed in section 3.2.4. The statistics of PM_{10} show much

Table 1. Comparison between the base case simulation results for O_3 and observations from the AQS network. (Obs. stands for observation. Sim. stands for simulation. Corr. stands for correlation, No. Sites means number of observation site used for statistics.)

Period	Obs. mean ppb	Sim. mean ppb	RMSE ppb	Corr. %	MNGB %	MNGE %	No. Sites
Summer	41.1	50.9	16.7	56.7	12.0	29.7	1262
Winter	27.3	33.9	10.4	51.4	8.8	23.1	664

Table 2. Comparison between simulation results for $PM_{2.5}$ and observations from the AQS network. (Obs. stands for observation; Sim. stands for simulation. Corr. stands for correlation; No. Sites means number of observation site used for statistics.)

Scenario	Period	Obs. mean $\mu g/m^{-3}$	Sim. mean $\mu g/m^{-3}$	RMSE $\mu g/m^{-3}$	Corr. %	MFB %	MFE %	No. Sites
Base	Summer	12.6	21.9	18.1	17.8	36.7	62.7	176
$\gamma=10^{-3}$	Summer	12.6	24.1	20.5	18.3	41.2	66.3	176
$\gamma=10^{-4}$	Summer	12.6	22.1	18.4	17.8	37.2	63.1	176
$\gamma=10^{-5}$	Summer	12.6	21.9	18.1	17.8	37.0	62.9	176
Base	Winter	12.3	13.0	11.4	31.3	2.8	60.9	166
$\gamma=10^{-3}$	Winter	12.3	12.6	11.1	31.4	0.6	60.4	166
$\gamma=10^{-4}$	Winter	12.3	12.9	11.4	31.4	2.4	60.8	166
$\gamma=10^{-5}$	Winter	12.3	13.0	11.4	31.3	2.7	60.9	166

closer agreement between the simulation results and the observations than $PM_{2.5}$, as shown on Table S2 in the SI, with the MEB values for each site mapped in Figure S4. The MFE is similar to that of $PM_{2.5}$, while much smaller MFB values are found for the summer. Similar to $PM_{2.5}$, the increase of NH_3 uptake coefficient leads to lower PM_{10} concentration for the winter, but higher PM_{10} concentration for the summer. One possible explanation for the different performance between $PM_{2.5}$ and PM_{10} could be the underestimation of coarse mode particle due to the mode-species limitation of CMAQ. Most of the SOA species are not allowed to grow into the coarse mode and their mass could be trapped in the accumulation mode therefore cause this overestimation.

Second, the simulated concentration of gas-phase NH_3 is compared to observation data from the Ammonia Monitoring Network (AMoN). In each AMoN site, samples are deployed for 2-week periods. Details about the network and its sampling method can be found on NADP (2014). Table 3 shows the statistics between each simulation case and the measurement data, and the MFB values for ammonia measured by individual stations are presented in Figure S5. The seasonal influence is quite clear in the statistics of the two base case simulations. Similar to the $PM_{2.5}$, the model overestimates the NH_3 concentration for the summer, especially over the southeast and the Central Valley regions of California. On the contrary, the simulated NH_3 concentration is underestimated for the winter. The impacts of different NH_3 uptake coefficients on NH_3 concentrations are consistent between the winter and the summer, the NH_3 concentration decreases as the uptake coefficient increases. However,

Table 3. Comparison between simulation results for NH_3 and observations from the AMoN network. (Obs. stands for observation; Sim. stands for simulation. Corr. stands for correlation; No. Sites means number of observation site used for statistics.)

Scenario	Period	Obs. mean $\mu g/m^{-3}$	Sim. mean $\mu g/m^{-3}$	RMSE $\mu g/m^{-3}$	Corr. %	MFB %	MFE %	No. Sites
Base	Summer	1.36	2.17	1.41	20.2	46.7	72.2	46
γ=10^{-3}	Summer	1.36	0.63	1.07	-26.1	-70.1	96.4	46
γ=10^{-4}	Summer	1.36	1.48	1.08	-2.0	7.3	63.2	46
γ=10^{-5}	Summer	1.36	1.30	1.30	18.1	38.0	68.9	46
Base	Winter	0.77	0.37	0.57	26.2	-63.3	88.7	19
γ=10^{-3}	Winter	0.77	0.31	0.60	29.7	-78.9	98.0	19
γ=10^{-4}	Winter	0.77	0.36	0.58	27.5	-65.9	90.1	19
γ=10^{-5}	Winter	0.77	0.37	0.57	26.5	-63.6	88.9	19

Table 4. Comparison between simulation results for NH_4^+ and observations from CSN network. (Obs. stands for observation; Sim. stands for simulation. Corr. stands for correlation; No. Sites means number of observation site used for statistics.)

Scenario	Period	Obs. mean $\mu g/m^{-3}$	Sim. mean $\mu g/m^{-3}$	RMSE $\mu g/m^{-3}$	Corr. %	MFB %	MFE %	No. Sites
Base	Summer	0.82	0.98	0.70	31.8	7.7	71.3	187
γ=10^{-3}	Summer	0.82	0.83	0.62	31.4	-5.3	70.3	187
γ=10^{-4}	Summer	0.82	0.92	0.66	32.0	3.2	70.5	187
γ=10^{-5}	Summer	0.82	0.96	0.69	31.9	6.8	71.1	187
Base	Winter	1.30	1.20	0.96	45.8	-12.8	64.5	187
γ=10^{-3}	Winter	1.30	1.08	0.93	45.1	-21.1	64.3	187
γ=10^{-4}	Winter	1.30	1.18	0.95	45.6	-14.1	64.4	187
γ=10^{-5}	Winter	1.30	1.20	0.96	45.8	-12.9	64.4	187

such impact is much more significant during the summer than the winter. Figure S6 in the SI section shows the difference of MFE between the base cases and cases with different assumed values for NH_3 uptake coefficients. For the winter cases, the overall impact on model performance is negligible. For the summer cases, improvements in model performance can be found in southeast and the Central Valley regions of California. The choice of the γ=10^{-4} appears to provide the greatest model performance improvement in the summer, based on both Table 3 and Figure S6.

Finally, simulation results of individual inorganic aerosol compounds (e.g., NH_4^+, SO_4^{2-}, and NO_3^-) are also compared with measurement data obtained from the EPA's Chemical Speciation Network (CSN). The CSN network collect 24-h integrated samples every day (midnight to midnight) of major fine particle chemical components and most of CSN sites are in urban areas. Detailed description of the network and its sampling protocol are available in Malm et al. (2004). The statistics for SO_4^{2-} presented in Table S3 of the SI section with the maps of MFB values for all individual sites (Figure S11) indicate good

Table 5. Comparison between simulation results for NO_3^- and observations from CSN network. (Obs. stands for observation; Sim. stands for simulation. Corr. stands for correlation; No. Sites means number of observation site used for statistics.)

Scenario	Period	Obs. mean $\mu g/m^{-3}$	Sim. mean $\mu g/m^{-3}$	RMSE $\mu g/m^{-3}$	Corr. %	MFB %	MFE %	No. Sites
Base	Summer	0.47	0.88	0.85	17.8	31.1	87.3	187
γ=10^{-3}	Summer	0.47	0.46	0.54	14.7	-38.2	90.1	187
γ=10^{-4}	Summer	0.47	0.70	0.68	18.2	10.3	80.6	187
γ=10^{-5}	Summer	0.47	0.84	0.81	18.1	27.6	85.8	187
Base	Winter	2.43	3.14	2.57	40.4	31.0	75.2	187
γ=10^{-3}	Winter	2.43	2.74	2.29	40.0	20.5	71.0	187
γ=10^{-4}	Winter	2.43	3.07	2.52	40.4	29.3	74.4	187
γ=10^{-5}	Winter	2.43	3.13	2.56	40.4	30.8	75.1	187

model performance. There is good agreement between mean observed and simulated concentrations with small MFB and MFE values that satisfy the model performance goals proposed by Boylan and Russell (2006) (|MFB| $\leq$ 30% and MFE $\leq$ 50%). The statistics of other scenarios are not presented in the table, as the change of NH_3 uptake coefficient shows no observable impact on the SO_4^{2-} statistics. This is due to the extremely low volatility of sulfuric acid, which forces almost the entire SO_4^{2-} to be condensed into the aerosol phase, regardless the concentration of NH_3.

For NH_4^+ (Table 4), in general, the statistics show a good model performance, as the MFB and MFE satisfied the model performance criteria proposed by Boylan and Russell (2006) in all 8 scenarios. Additionally, Figure S7 in the SI section shows the level of bias (MFB) of individual CSN sites for the base case, which shows NH_4^+ is considerably overestimated over the southeast but underestimated in the midwest regions of the country for both winter and summer. Based on Table 4, the NH_4^+ is slightly overestimated in the base case for the summer period, however, the addition of NH_3 uptake leads to a lower modeled NH_4^+ concentration and reduced level of overestimation. Such improvements happen over most of the eastern US as well as the Central Valley of California, based on Figure S8 (b) and (d) in the SI which presents the difference in MFE between the base cases and cases with NH_3 uptake coefficients. Similar to NH_3, the γ=10^{-4} case shows better model performance improvement than the γ=10^{-3} case in the summer. For the winter, the NH_4^+ concentration is slightly underestimated in the base case, so the decrease of NH_4^+ concentration caused by the increase of NH_3 uptake coefficient leads to an even larger underestimation. As shown on Figures S8 (a) and (c), model performance is not improved in most of the stations, except over the southeast region.

Table 5 gives the statistics for NO_3^-. In general, the model over estimates the NO_3^- concentration for both periods, and a poor correlation is found for the summer. The relatively poor model performance with respect to NO_3^- is consistent with previous CMAQ studies (Eder and Yu, 2006; Appel et al., 2008). The addition of NH_3 uptake coefficient reduces the simulated NO_3^- concentration significantly. The γ=10^{-3} case leads to a mean NO_3^- concentration which is much closer to the observed average than the base case in both simulated periods. Figure S9 in the SI section shows the maps of MFB values for particulate nitrate measured by each station in the base cases. We find that the modeled NO_3^- is overestimated over the southeast region for both periods, and also overestimated along the Central Valley of California during the summer period. The addition of NH_3 uptake reduced such overestimation and improved the model performance in those regions as shown in Figure S10, which presents the difference of MFE between base cases and cases with different NH_3 uptake included. For the winter period, it is clear the γ=10^{-3} case provides better model performance. For the summer period, the model performance improvement occurred on more observation sites in the γ=10^{-4} case than the γ=10^{-3} case. However, the γ=10^{-3} case provides better improvement at some sites, although more sites suffer performance deterioration compares to the γ=10^{-4} case. In summary, the model tends to preformem better on the whole with NH_3 uptake in SOA included with $\gamma \sim 10^{-3}$ to 10^{-4}.

3.2 Air Quality Impacts

3.2.1 Impact on gas-phase NH_3 and HNO_3 concentrations

Figure S12 in the SI section shows the time series of daily domain-averaged (averaged over 24 hours and the simulation domain) NH_3 for both the winter and summer, for different uptake coefficient values. In general, the NH_3 concentration is reduced after the introduction of the SOA-based NH_3 uptake process. The magnitude of the reduction is increased as the uptake coefficient increases. For the winter, the spatial-time-averaged (averaged over entire period and the simulation domain) NH_3 concentration for the base case is 0.44 ppb, while the value decreases to 0.43 ppb (-2.3 %) for the γ=10^{-5} case, 0.41 ppb (-6.8 %) for the γ=10^{-4} case and 0.31 ppb (-29.5 %) for the γ=10^{-3} case. For the summer, the spatial-time-averaged NH_3 concentration for the base case is 2.30 ppb, while the value decreases to 2.10 ppb (-8.7 %) for the γ=10^{-5} case, 1.58 ppb (-31.3 %) for the γ=10^{-4} case and 0.76 ppb (-67.0 %) for the γ=10^{-3} case. The impact of the uptake process is higher for the summer due to larger SOA concentrations during the summer (spatial-time-averaged 9.25 μg/m^{-3} for the base case) than the winter (spatial-time-averaged 2.72 μg/m^{-3} for the base case).

The spatial distribution of the impact over the simulated domain is also investigated. Figure 1 (a), (c) shows the time-averaged spatial distribution of NH_3 for the winter and summer base cases, while the differences between the γ=10^{-3} case and the base case are shown in Figure 1 (b), (d). For both periods, the central valley of California is a hot spot for NH_3 emissions, and the region exhibits the most significant impact due to the introduction of the new NH_3 uptake mechanism. This is due to the intensive agricultural activities in this region including the heavy application of fertilizers (Krauter et al., 2002), and the year-round farming pattern supported by California's relatively warm climate. The hog farm industry is largely responsible for the high NH_3 concentration, in North Carolina and north Iowa in the summer, where significant NH_3 loss can also be spotted in the γ=10^{-3} case. Agriculture and wild fires also produce some hot spots of ammonia concentration in others areas, such as southern Florida in the winter and several locations in northern California and Washington states, where NH_3 concentrations also decreased significantly in the γ=10^{-3} case. The spatial distribution of differences between the base case and the γ=10^{-4} and γ=10^{-5} cases are similar to the γ=10^{-3} only with different scales. These differences are shown in Figure S13 of supporting information.

As the condensation of HNO_3 into the particle phase is directly associated with NH_3 concentration, it is reasonable to infer that the introduction of the NH_3 uptake mechanism could also impact the concentration of HNO_3. Figure S14 in the SI shows

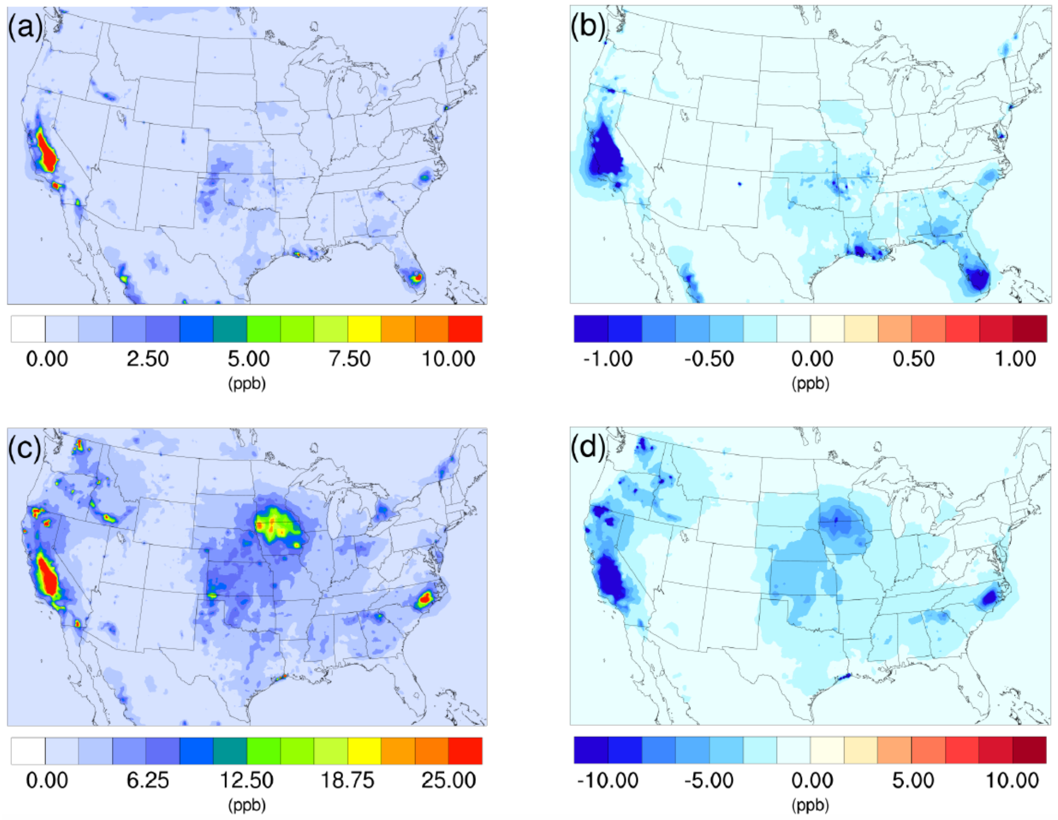

Figure 1. Spatial distribution of time-averaged NH_3 concentrations in the base case for (a) winter, and (c) summer. Spatial distribution of the difference in time-averaged NH_3 concentrations between the γ=10^{-3} case and the base case for (b) winter, and (d) summer. Negative values represent decreases in concentration with respect to the base case.

the time series of daily averaged HNO_3 for both the winter and summer. In contrast to NH_3, the integration of the NH_3 uptake mechanism leads to an increase in HNO_3 concentration, and the scale of magnitude of the increase rises as the uptake coefficient is increased, although its scale of variation is much smaller than that of NH_3. For the winter, the difference between the base case and the γ=10^{-5} case is very small ($<$ 0.2 %), and remain insignificant for the the γ=10^{-4} case ($\sim$ 1.2 %). Only the γ=10^{-3} case shows an significant increase in HNO_3 as concentrations increase by 8.5 % (the spatial-time-averaged concentration is 0.27 ppb for the base case and 0.30 ppb for the γ=10^{-3} case). Similar to the NH_3 variation, the impact becomes larger for the summer, where the spatial-time-averaged HNO_3 concentration for the base case is 0.51 ppb, while the value increases by 2.0 % (0.52 ppb) for the γ=10^{-5} case, 7.8 % (0.55 ppb) for the γ=10^{-4} case and 19.6 % (0.61 ppb) for the γ=10^{-3} case. These increase in HNO_3 concentrations are due to the reduction in NH_3 caused by the conversion of NH_3 into NOC, making less NH_3 available for reaction with HNO_3 to form the particle phase NH_4NO_3.

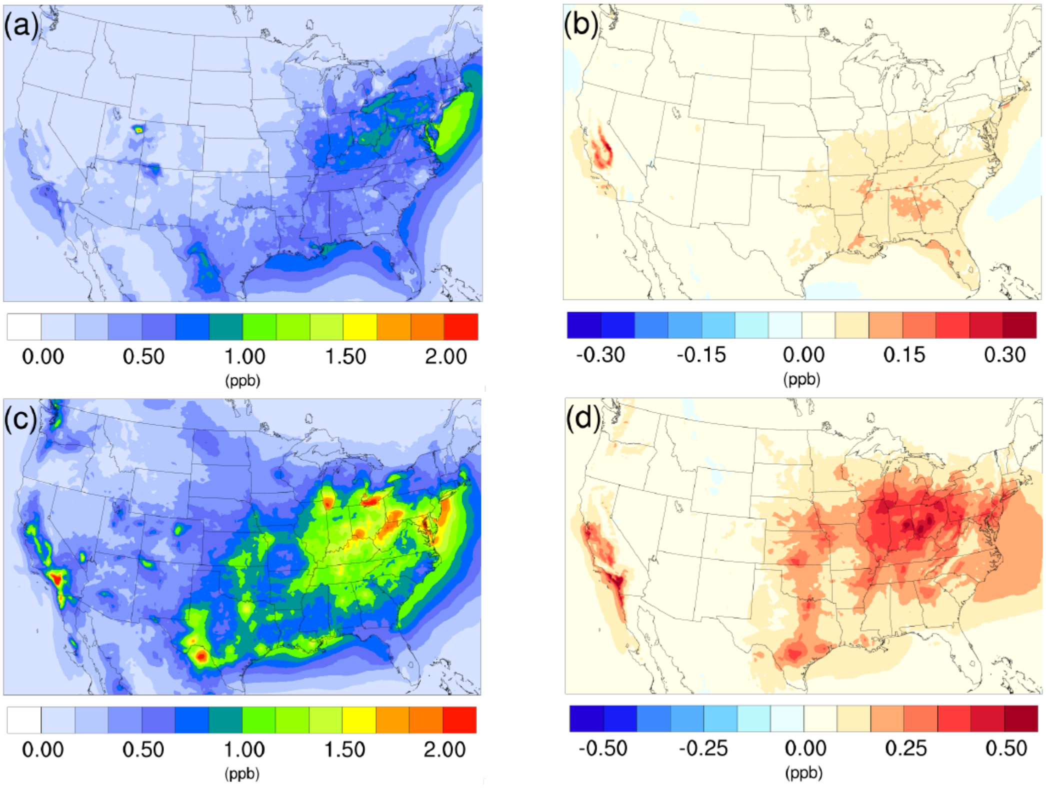

Figure 2. Spatial distribution of time-averaged HNO_3 concentrations in the base case for (a) winter, and (c) summer. Spatial distribution of the difference in time-averaged HNO_3 concentrations between the γ=10^{-3} case and the base case for (b) winter, and (d) summer. Positive values represent increases in concentration with respect to the base case.

The time averaged spatial distributions of HNO_3 for both the winter and summer base cases are presented in Figure 2 (a) and (c). The north-east region exhibits relatively high HNO_3 concentration for both periods, largely due to the high NO_x (NO + NO_2) emissions from transportation activities. The addition of NH_3 uptake process does not cause an obvious impact in this region for the winter, as the reduction of NH_3 is very small (Figure 1 (b)) due to low SOA and NH_3 concentrations in the base case. In contrast, the increase of HNO_3 becomes much more significant for this region in the summer, as the loss of NH_3 becomes greater due to larger NH_3 and SOA concentrations in the base case. The winter hot spot around northeastern Utah (Uintah Basin) could be caused by the stagnant atmospheric conditions during the winter in the valley (Lee et al., 2014), which traps NO_x emitted from local and remote sources located on the east side of the valley. The resulting NOx undergoes a nighttime reaction with O_3 forming N_2O_5 (high N_2O_5 concentration is spotted in the model at the same place as shown on Figure S24). Additionally, the lack of NH_3 also favors the HNO_3 accumulation, as a result, the addition of NH_3 does not have much impact on this spot. The largest increase in HNO_3 concentrations in winter is found over the central valley of California, which also corresponds to the largest NH_3 reduction (Figure 1 (b)). For the summer, the largest impact occurs over the hot spot of southern California, where strong traffic emissions of NO_x and active photo-chemistry provide strong HNO_3 source. The significant reduction of NH_3 concentration from the south central valley could reduce the potential sink of HNO_3 into particle-phase and leave more HNO_3 in the gas-phase. The spatial distribution of differences between the base case and the γ=10^{-4} and γ=10^{-5} cases are similar to the γ=10^{-3} only with different scales, and they can be found in the SI (Figure S15).

3.2.2 Impact on inorganic PM

One of the effects of the gas-phase NH_3 reduction due to the inclusion of SOA-based NH_3 conversion to NOC would be the decrease of NH_4^+ concentration in the particle phase, as all NH_4^+ originates from gas phase NH_3. Figure S16 in the SI shows the time-spatial evolution of daily averaged NH_4^+ for the winter and the summer. In general, the addition of NH_3 uptake in the model causes a decrease in particle phase NH_4^+ concentration, and the impact is more significant for the summer than the winter. For summer case, the average decrease in $NH_4^+$is 1.8 % for γ=10^{-5}, 10.7 % for γ=10^{-4} and 28.2 % for γ=10^{-3}; for winter case, the averaged decrease is 0.2 % for γ=10^{-5}, 2.3 % for γ=10^{-4} and 13.2 % for γ=10^{-3}. Such behavior corresponds well to the level of NH_3 reduction in Figure S12, and is caused by the higher SOA concentrations during the summer.

The time-averaged spatial distributions of the NH_4^+ concentration for both the winter and summer base case are shown on Figure 3 (a) and (c). Most of the NH_4^+ is concentrated over the eastern part of the US, as a result of high NH_3 concentrations (see Figure 1) in this region combined with the abundance of NH_3 neutralizers (e.g., HNO_3 and H_2SO_4). Another hot spot is the Central Valley of California and the South Coast Air Basin of California (Nowak et al., 2012), resulting from high NH_3 emissions from the intensive agriculture (Figure 1). In presence of both HNO_3 and H_2SO_4, NH_3 is first neutralized by H_2SO_4 to form either $(NH_4)_2SO_4$ or NH_4HSO_4 in the particle phase, while the rest of the NH_3 reacts with HNO_3 and forms particle phase NH_4NO_3. The percentage of NH_4^+ associated with NO_3^-, SO_4^{2-} and HSO_4^- could be investigated by comparing the spatial distribution of the NO_3^- concentration for corresponding period in Figure 4 (a) (c) and the SO_4^{2-} in Figure 5 (a) (b). For the winter, the H_2SO_4 concentration is insufficient to neutralize all the NH_3 for the mid-east region, so more NO_3^- is involved in the NH_3 neutralization, and there are more nitrate particles than sulfate particles. For the summer, as the sulfate concentration almost doubles over the mid-east US compares to the winter, most of the NH_3 is neutralized by H_2SO_4. This causes a absence of NO_3^- above this region, and only appears on the surrounding region where sulfate concentration is low. For the West Coast and the Central Valley of California, the enriched NH_4^+ mostly exists in the form of NH_4NO_3, as the sulfate concentration is low in this region for both periods. Figure 3 (b) and (d) present the spatial distribution of the difference in NH_4^+ concentration between the γ=10^{-3} case and the base case, which is highly correlated with the NH_3 variation map (Figure 1). The reduction in NH_3 due to the SOA uptake, directly impacts the available NH_3 that could be condensed into the particle phase, and reduces the NH_4^+ concentration consequently. The spatial distribution of differences between the base case and the γ=10^{-4} and γ=10^{-5} cases is similar to the γ=10^{-3} only with different scales, as shown in Figure S17 in the SI.

The concentration of NO_3^- also changes as a result of adding the NH_3 conversion into NOC. Figure S18 in the SI shows the variation in daily-spatial averaged NO_3^- concentration under different scenarios for both the winter and summer. Overall, adding the NH_3 uptake mechanism leads to a decrease in NO_3^- concentrations for both periods. Similar to NH_4^+, the impact is more significant for the summer than the winter. The average reductions for the winter are 0.2 % for γ=10^{-5}, 1.9 % for

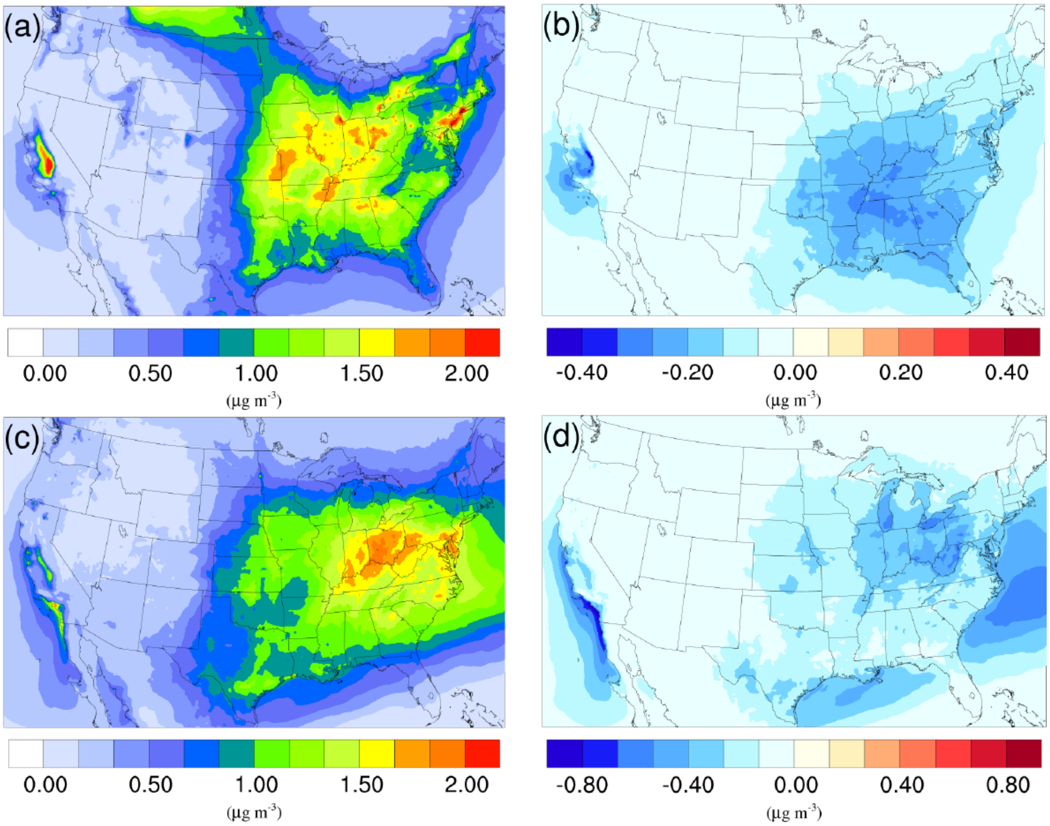

Figure 3. Spatial distribution of time-averaged NH_4^+ concentrations in the base case for (a) winter, and (c) summer. Spatial distribution of the difference in time-averaged NH_4^+ concentrations between the γ=10^{-3} case and the base case for (b) winter, and (d) summer. Negative values represent decreases in concentration with respect to the base case.

γ=10^{-4} and 10.9 % for γ=10^{-3}. For the summer, the average reductions are 1.9 % for γ=10^{-5}, 10.6 % for γ=10^{-4} and 24.3 % for γ=10^{-3}. Such variations are similar to those of NH_4^+, where the γ=10^{-5} case in the summer has similar reductions to γ=10^{-4} case in the winter. And the magnitude of the difference is also close to the difference in NH_4^+, indicating almost all the NH_4^+ reduction is from NH_4NO_3.

The spatial distributions of the NO_3^- variation due to the addition of the NH_3 uptake mechanism (γ=10^{-3}) are presented in Figure 4 (b) (d) for the winter and summer. By comparing with the base cases (see Figure 4 (a) (c)), it is clear that most of the NO_3^- reduction occurs over regions with high NO_3^- concentration, such as the Central Valley of California, the South Coast Air Basin of California and vast regions over the mid-east US. One exception is the high NO_3^- region over Canada on the north edge of Montana and North Dakota during the winter. Neither NH_4^+ concentration nor NO_3^- concentration changes much, mostly because the SOA concentration is extremely low for that region (see Figure 6 (a)), so almost no NH_3 is lost due

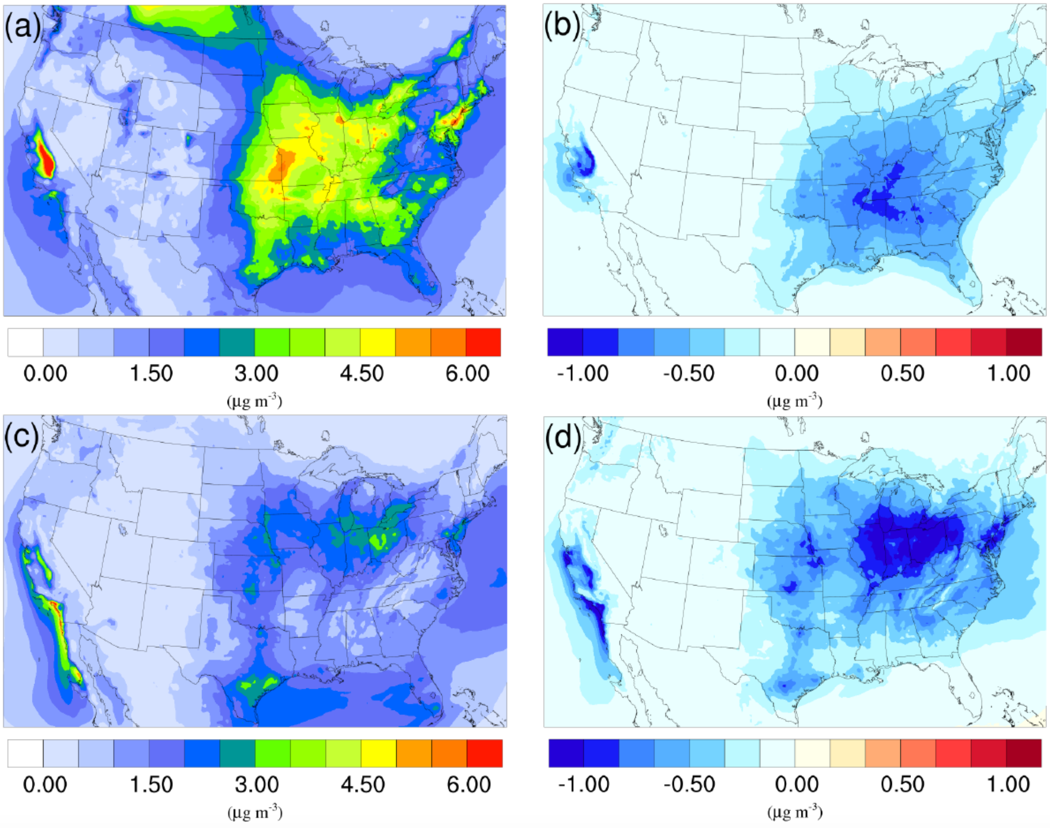

Figure 4. Spatial distribution of time-averaged NO_3^- concentrations in the base case for (a) winter, and (c) summer. Spatial distribution of the difference in time-averaged NO_3^- concentrations between the γ=10^{-3} case and the base case for (b) winter, and (d) summer. Negative values represent decreases in concentration with respect to the base case.

to the SOA uptake. The same occurs in south Florida during the summer. The spatial distribution of differences between the base case and the γ=10^{-4} and γ=10^{-5} cases is similar to the γ=10^{-3} only with different scales, shown in Figure S19 of the SI.

3.2.3 Impact on organic PM

Figure 6 (a), (c) shows the time-averaged spatial distribution of SOA for the winter and summer base cases. For both seasons, high SOA concentrations are found over the southeastern US due to high vegetation coverage in this region, while hot spots in the northwestern region are caused by widespread fire events. The averaged SOA concentration is more than 3 times higher in the summer case (9.25 μg m^{-3}) than in the winter (2.72 μg m^{-3}), largely due to the much higher biogenic SOA concentrations (4.43 μg m^{-3} summer vs. 0.22 μg m^{-3} winter) resulting from elevated biogenic emissions in the warm season.

As mentioned in section 2, the NH_3 uptake parameterization used in this study does not directly add mass to SOA because the original SOA carbonaly and the NOC they convert into have similar molecular weight. However, significant changes in

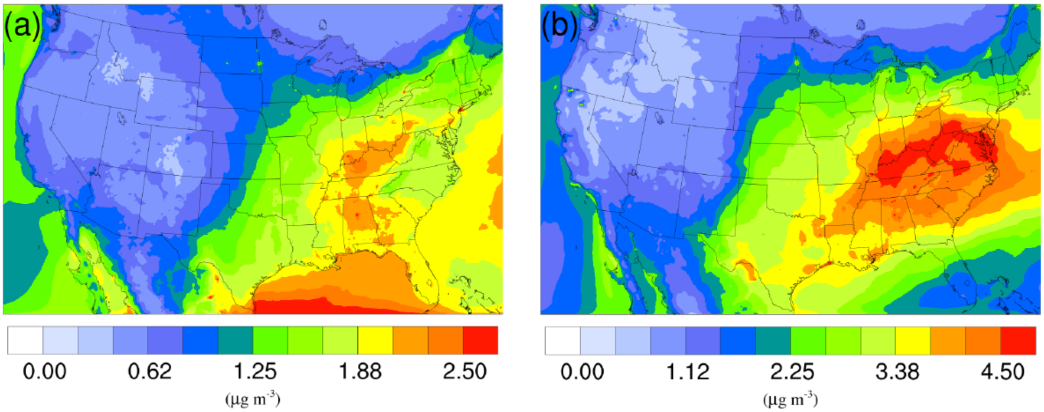

Figure 5. Spatial distribution of time-averaged SO_4^{2-} concentrations in the base case for (a) winter, and (b) summer. The difference due to NH_3 conversion into NOC is not shown because it is very small.

SOA concentration are observed after implementing the NH_3 uptake mechanism, which is indirectly caused by the changes in particle acidity (see below). As demonstrated in Figure 6 (b), (d), implementing the NH_3 uptake mechanism has a significant impact on the SOA concentrations during the summer, but has almost no impact on SOA for the winter. Almost the entire increase in SOA concentrations in the summer is due to the mass change in biogenic SOA (BIOSOA) (see Figure 7 (a) and 6 (d), their average concentrations for the base case are in the SI Figure S20). Further investigation reveals that the majority of the increase ($\sim$ 80%) is caused by the nonvolatile AISO3 species (7 (b)), which is the isoprene epoxydiols (IEPOX) derived SOA through the acid-catalyzed ring-opening reactions (Pye et al., 2013). This increase in AISO3 is caused by the increase of aerosol aqueous phase acidity due to the reduction in NH_4^+ after adding the NH_3 conversion into NOC. This increase in particle acidity corresponds well with the sensitivity study between NH_3, SO_4^{2-} and particle pH presented in Figure 2 of Weber et al. (2016), where particle pH is found to be more sensitive to NH_3 concentrations than to SO_4^{2-} concentrations. Figure 7 (c) shows a large drop in pH value ($\sim$0.9 - 2.3) (pH change for other scenarios are shown in SI Figure S21) in the southeast region where the increase of the AISO3 is most significant and there is a simultaneous decrease in IEPOX concentrations (Figure 7 (d)). The largest pH variation appears over the northwest region. However, there is no observable impact on SOA concentrations due to the extremely low concentration of both isoprene and IEPOX (see Figure 7 (e) and (f)) in this area. Moreover, the reduction in NH_4^+ concentrations also increases the ratio of SO_4^{2-}/HSO_4^-, where SO_4^{2-} can acts as a nucleophile and promote the IEPOX uptake process. This also contributes to the increase of AISO3 in the γ=10^{-3} case.

Figure 8 shows the time evolution of daily-spatial averaged H^+, IEPOX and AISO3 for both the winter and summer. Although the average H^+ concentration in the base case is similar between two periods, the variation is much smaller for the winter largely due to the lower SO_4^{2-} concentrations in the winter which restraints the acidity variation level. Additionally, lower SOA concentrations in winter also reduces the magnitude of NH_4^+ variation. As a result, addition of the NH_3 uptake mechanism does not have large impact on the AISO3 concentration for most of the simulation (except for the last several

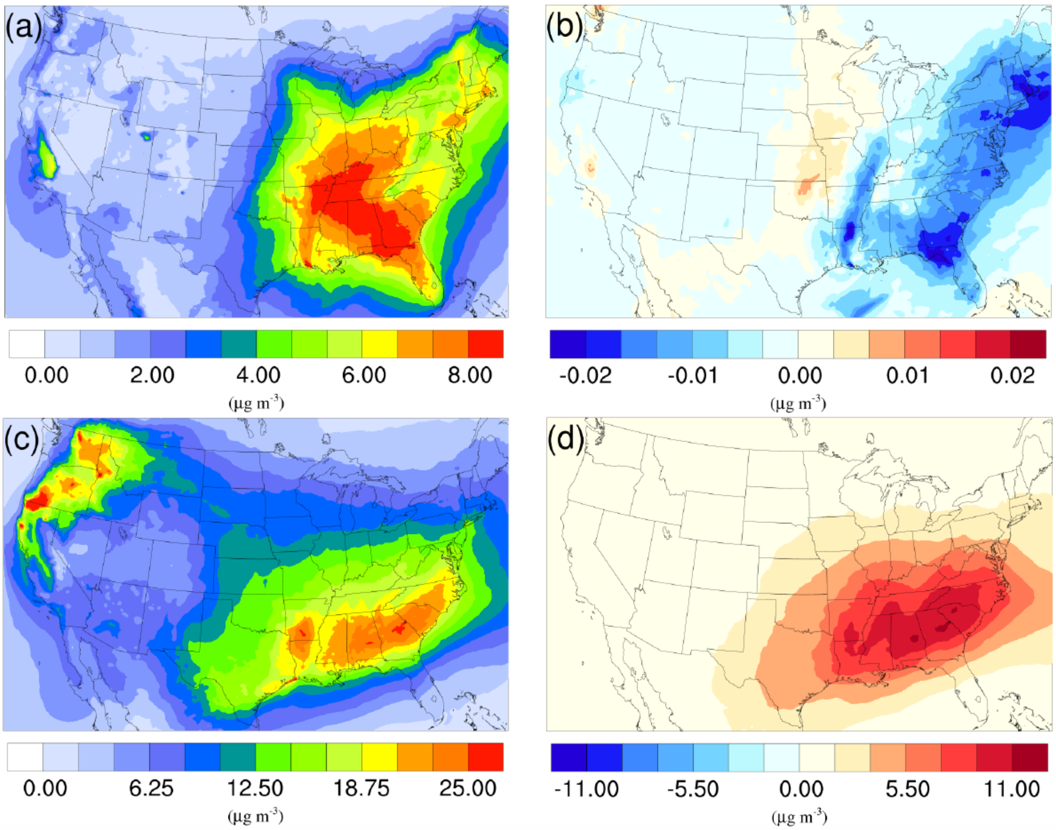

Figure 6. Spatial distribution of time-averaged SOA concentrations in the base case for (a) winter, and (c) summer. Spatial distribution of the difference in time-averaged SOA concentrations between the γ=10^{-3} case and the base case for (b) winter, and (d) summer. Positive values represent increases in concentration with respect to the base case, and negative values represent decreases in concentration with respect to the base case.

days). On the contrary, the summer shows a significant increase in H^+ concentrations as the NH_3 uptake coefficient increases, while the concentration of IEPOX decrease. And the increase of AISO3 concentration is remarkable, with more than ten times growth on average between the γ=10^{-3} case (1875.2 ng m^{-3}) and the base case (181.75 ng m^{-3}). The amount of growth on AISO3 seems linear with different value of the NH_3 uptake coefficient (γ=10^{-5}: 16.2%; γ=10^{-4}: 171.9%; γ=10^{-3}: 931.6%).

Beside the isoprene epoxydiols pathway, other biogenic SOA species contribute the rest of the SOA changes (20%), including other SOA species derived from isoprene (AISO1 and AISO2), from monoterpenes (ATRP1 and ATRP2), from sesquiterpenes (ASQT), and AOLGB which represents the aged nonvolatile SOA origin from AISO1, AISO2, ATRP1, ATRP2 and ASQT. The common point with those SOAs (AISO1, AISO2, ATRP1, ATRP2 and ASQT) are that they all have a pathway to be formed through the oxidation between gas phase NO_3 radicals and their gas precursors. One possible explanation could be

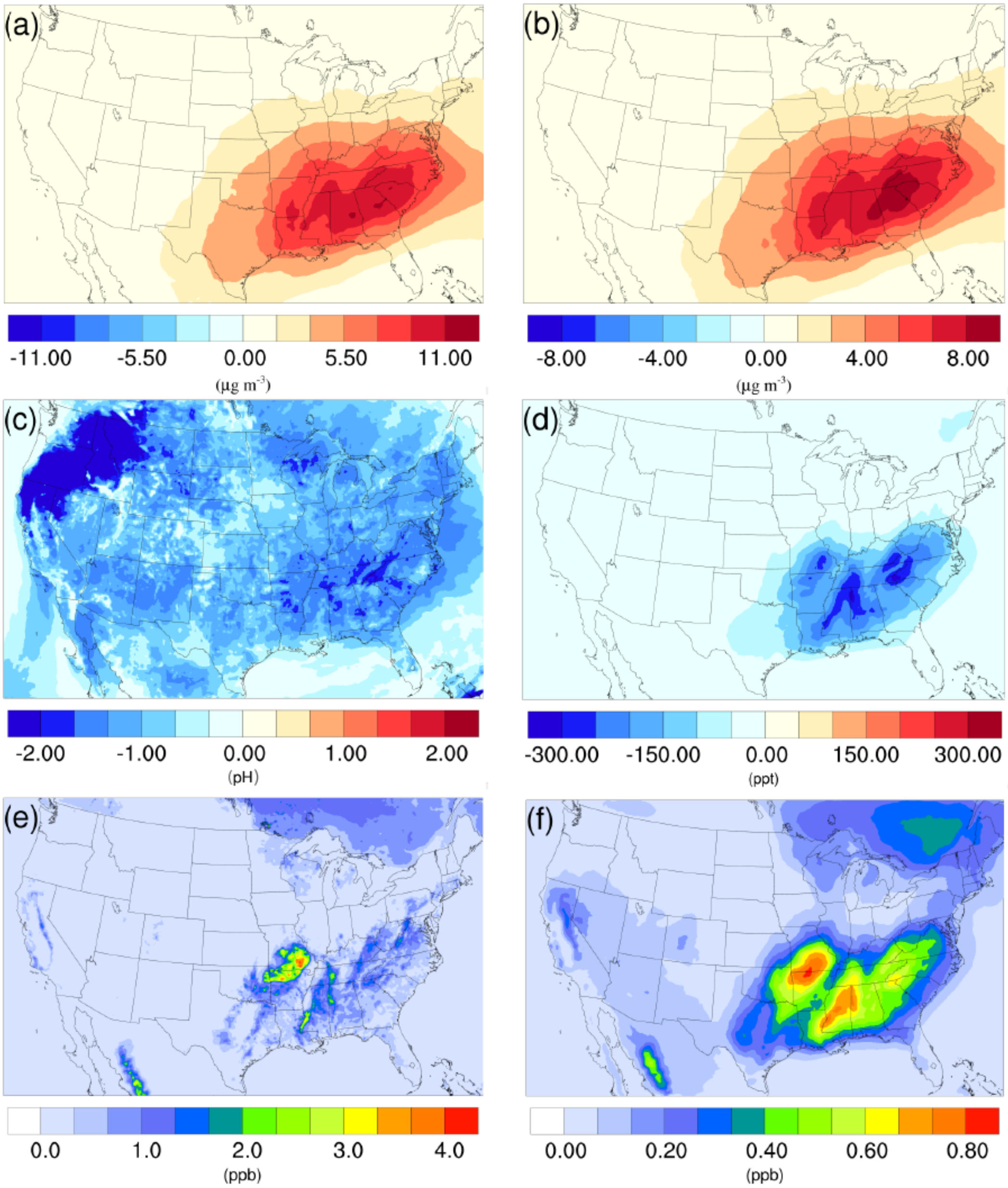

Figure 7. Spatial distribution of the difference in time-averaged (a) biogenic SOA concentrations, (b) isoprene epoxydiols (IEPOX) derived SOA concentrations, (c) particle acidity (pH), and (d) isoprene epoxydiols concentrations between the γ=10^{-3} case and the base case during the summer. Spatial distribution of time-averaged (e) isoprene, and (f) isoprene epoxydiols concentration in the base case during the summer.

that the addition of NH_3 uptake leads to an increase of gas phase HNO_3, which could shift the reaction balances between NO_3 and HNO_3 and leave more NO_3 available for SOA oxidation.

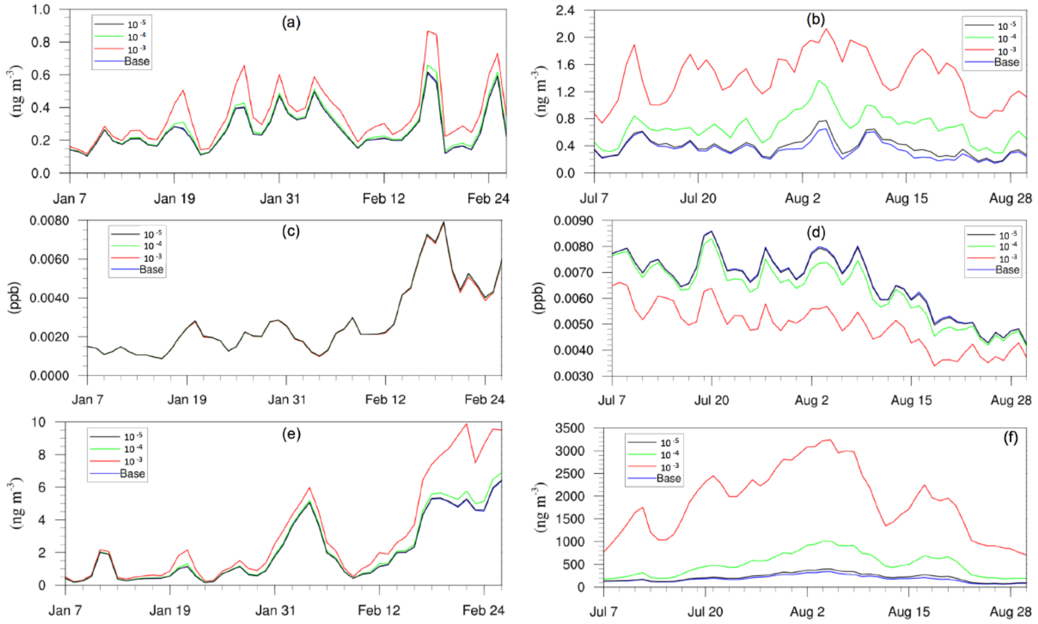

Figure 8. Daily, spatially-averaged concentrations of (a) particle phase H^+ in winter, (b) particle phase H^+ in summer, (c) isoprene epoxydiols in winter, (d) isoprene epoxydiols in summer, (e) isoprene epoxydiol derived SOA in winter, and (f) isoprene epoxydiol derived SOA in summer.

3.2.4 Impact on total PM

Figure S22 in the SI presents the time evolution of daily-averaged concentrations of $PM_{2.5}$ and PM_{10} in different scenarios during both periods. First, both the pattern and level of impact caused by the NH_3 uptake mechanism is similar for $PM_{2.5}$ and PM_{10}, which indicates that most of the mass change due to this process occurs on fine particles. Secondly, the level of impact on both $PM_{2.5}$ and PM_{10} is much more significant over the summer than the winter, which is consistent with previous analysis of individual species. Third, opposite impact patterns are found between the winter and summer. The inclusion of NH_3 uptake mechanism leads to a decrease in the total PM mass for the winter, that is caused by the reduction of inorganic NH_4^+ and NO_3^- due to the decrease of NH_3 concentration, as detailed in section 3.2.2. On the contrary, PM concentrations during the summer increases after adding the NH_3 uptake mechanism. Although the concentration of inorganic species still decreases during the summer, the increase in biogenic SOA concentration, as detailed in section 3.2.3, outpaces the decrease caused by inorganic species and leads to an overall increase in total PM mass for the summer. For the winter, the average $PM_{2.5}$ concentration reduction is 0.07% for the γ=10^{-5} case, 0.59% for the γ=10^{-4} case and 3.39% for the γ=10^{-3} case. For the summer, the average $PM_{2.5}$ concentration increase is 0.14% for the γ=10^{-5} case, 2.05% for the γ=10^{-4} case and 12.38% for the γ=10^{-3} case.

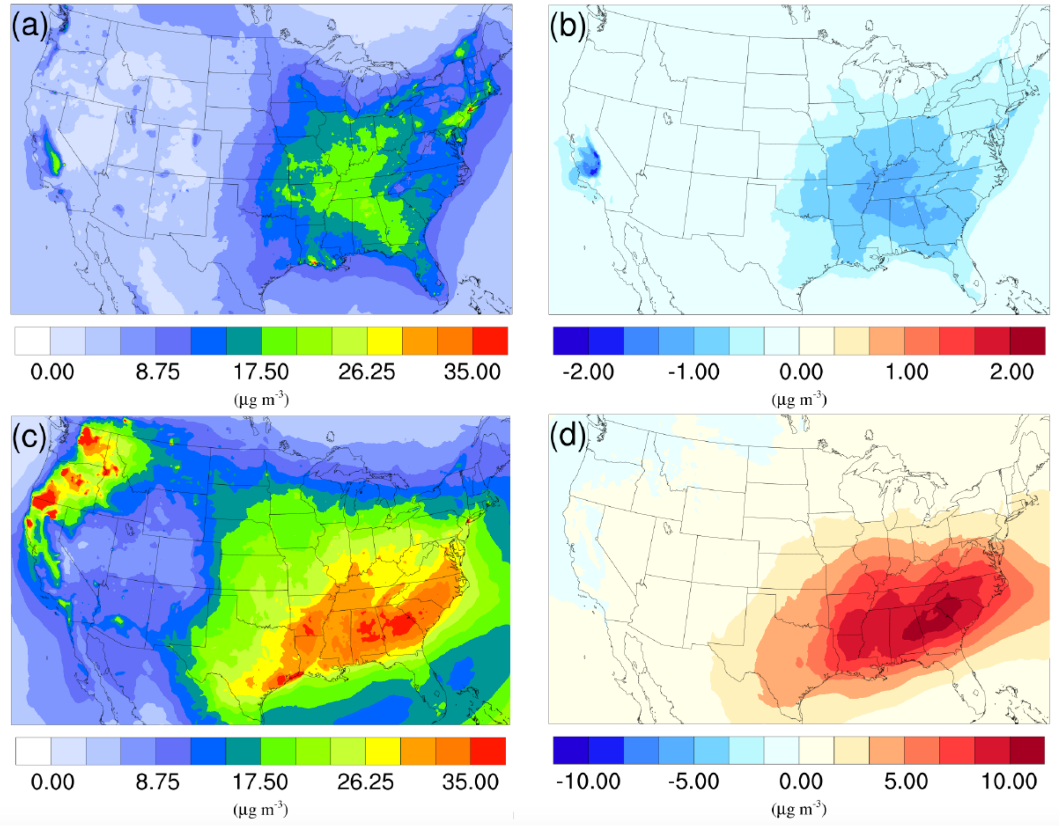

Figure 9. Spatial distribution of time-averaged $PM_{2.5}$ concentrations in the base case for (a) winter, and (c) summer. Spatial distribution of the difference in time-averaged $PM_{2.5}$ concentrations between the γ=10^{-3} case and the base case for (b) winter, and (d) summer. Positive values represent increases in concentration with respect to the base case, and negative values represent decreases in concentration with respect to the base case.

The spatial distribution of time averaged $PM_{2.5}$ concentration for the winter and summer is presented in Figure 9 (a) and (c) respectively. Most of the high $PM_{2.5}$ concentration happens over the mid-east US during the winter, with additional hot spots over the Central Valley of California, resulting in an overall average of 7.47 $\mu g/m^3$. $PM_{2.5}$ concentrations are highly correlated with the population density map of the US, indicating a dominant anthropogenic origin. The relatively low fraction of biogenic SOA in winter also supports this point (Figure 10 (a)). The model predicts a much higher $PM_{2.5}$ concentration for the summer, with an average concentration of 16.17 $\mu g/m^3$. The hot spots observed over the northwest of the country and coastal area over southeast Texas are caused by wild fire events. In general, high $PM_{2.5}$ concentration over the southeast of the US, where high fractions of biogenic SOA are found (Figure 10) (b). This could be a result of both high average temperatures during the summer and high vegetation density in that region. Figure 9 (b) shows the variation in $PM_{2.5}$ concentrations between the γ=10^{-3} case and the base case for the winter. An overall reduction can be observed from the map, with the highest reduction

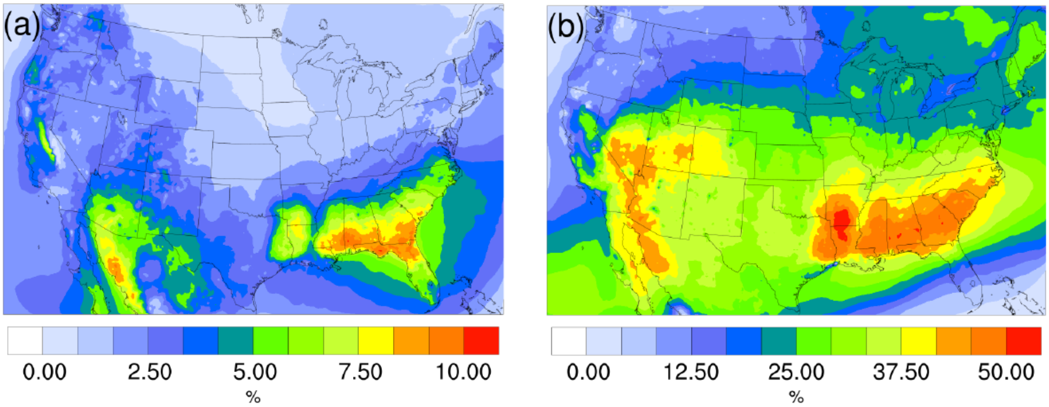

Figure 10. Spatial distribution of time-averaged biogenic SOA fraction of total $PM_{2.5}$ for (a) the winter, and (b) summer.

around the Central Valley of California and a smaller reduction over the vast mid-east region. This is mostly caused by the decrease of NH_4NO_3 due to the reduction of gas-phase NH_3 concentrations as discussed in section 3.2.2. For the summer, although the decrease still appears over the northwest of the country, the prominent feature becomes a significant increase in $PM_{2.5}$ concentrations over the southeast region. This is due to the increase in biogenic SOA resulting from the enhanced acid-catalyzed ring-opening reactions as detailed in section 3.2.3.

4 Conclusions

In this study, the potential air quality impacts of the heterogeneous uptake of NH_3 by SOA accompanied by formation of NOC is investigated with the CMAQ model. Simulations over the continental US are performed for the winter and summer seasons of 2011 with a range of NH_3 uptake coefficients reported in the literature. First, the simulation results for the two base case simulations are compared with observation data from different monitoring networks, and statistics show an overall good model performance for most of the criteria. The inclusion of the SOA-based NH_3 conversion into NOC has a significant impact on the statistics of NH_3, NH_4^+, NO_3^-, but does not affect O_3 and SO_4^{2-}. The overestimation of NH_3 and NH_4^+ for the summer is reduced by this new mechanism. Moreover, the prediction of NO_3^- is improved by this mechanism, given that the overestimation of NO_3^- concentration gradually subsides as the uptake coefficient increases.

The comparison between different uptake coefficient scenarios and the base case allows a more detailed understanding of the impact of this mechanism on both gas phase and particle phase species. Simulation results indicate a significant reduction in gas-phase NH_3 due to conversion of NH_3 into NOC, and such reduction increases dramatically as the uptake coefficient increases. The highest spatially-averaged reduction in gas-phase NH_3 is 31.3 % in the winter and 67.0 % in the summer. This analysis is based on a range of uptake coefficient that span those reported in the literature. However, the actual value for each individual SOA could be lower or higher than the uniform uptake coefficient used in this study, although the magnitude of the impact still indicates the importance of including this process in air quality models. The seasonal differences are obvious as the impact is much more significant in the summer than in the winter, due to much higher NH_3 and SOA concentration in the summer. The concentration of gas-phase HNO_3 is also impacted by this new mechanism. As the NH_3 concentration drops because it is being converted into NOC, less HNO_3 is neutralized by NH_3, resulting in an overall increase in HNO_3 concentration. Such increases can be as high as 8.5% in the winter and 19.6% in the summer for the largest uptake coefficient. Geographically, the biggest reduction in NH_3 happens in the Central Valley of California during both seasons, the same location as the biggest increase in HNO_3 in the winter. While for the summer, HNO_3 increases more dramatically over the South Coast Air Basin of California and the northeast region of the country.

PM concentrations are found to decrease during the winter period, largely due to the reduction in ammonium nitrate formation causes by the decrease in gas-phase ammonia. The largest uptake scenario (γ=10^{-3}) leads to a 13.2% reduction of NH_4^+, 10.6% reduction of NO_3^- and 3.4% reduction of $PM_{2.5}$ in the winter. The most significant reduction also happens over the Central Valley of California region with a highest $PM_{2.5}$ drop of 2.0 $\mu g/m^3$. On the other hand, PM concentrations are found to increase during the summer due to the increase in biogenic SOA production resulting from the enhanced acid-catalyzed ring-opening reactions. Although the reduction in ammonium nitrate is even larger in magnitude during the summer (28.2% reduction in NH_4^+, 24.3% reduction in NO_3^-) than the winter, the dramatic increase in biogenic SOA outpaced the decrease caused by ammonium nitrate to result in an overall increase in total PM (12.4% increase in $PM_{2.5}$). Most of the biogenic SOA increases occur over the southeast region of the US, where high vegetation density is located. The average increase in biogenic SOA is 0.9% for γ=10^{-5}, 9.2% for γ=10^{-4} and 49.0% for γ=10^{-3}. For the species (AISO3) that is responsible for most of the increase, the γ=10^{-3} case leads to a 10-fold increase in concentration compared to the base case.

Results of this study show that the chemical uptake of NH_3 by SOA can have significant impact on the model-predicted concentration of important atmospheric pollutants, including NH_3, HNO_3, NH_4^+, NO_3^- and biogenic SOA. The impact on the total PM has a distinct pattern on different seasons. Future laboratory studies should be conducted to identify the nature of the chemical reaction between NH_3 and SOA species to provide more accurate model representation of the uptake process. Furthermore, better knowledge abut basicity of NOC is needed to verify whether they can neutralize inorganic acids. For example, single particle measurements conducted by Neuman et al. (2003) showed that organic aerosols also contributed to increases in fine-particle mass in regions with high NH_3 emissions rates, suggesting that NH_3 uptake can increase organic aerosol mass concentrations directly. Current air quality models only include one pathway for the acid-catalyzed SOA generation (based on the high NO_x case in the study of (Pye et al., 2013)), and a more detailed representation of other acid-catalyzed pathways could lead to even larger impact on the SOA concentration.

Code and data availability. Simulation result data sets are available upon request as they are too big to upload online (812 Gigabyte). The original CMAQ (version 5.2) code for the base case simulation is available on the CMAS website: https://www.cmascenter.org/cmaq/. The updated CMAQ code including the NH_3 uptake mechanism is available under the following link: http://albeniz.eng.uci.edu/software/CMAQv5.2_ withNH3Uptake.zip. CMAQ have a GNU (General Public License). The user can redistribute them and/or modify them under the terms of the GNU General Public License as published by the Free Software Foundation.

Competing interests. The authors declare that they have no conflict of interest.

Acknowledgements. This publication was developed under Assistance Agreement No. EPA 83588101 awarded by the U.S. Environmental Protection Agency to the Regents of the University of California. It has not been formally reviewed by EPA. The views expressed in this document are solely those of the authors and do not necessarily reflect those of the Agency. EPA does not endorse any products or commercial services mentioned in this publication. We also express our gratitude for UCI HPC assistance and especially Dr. Harry Mangalam and Garr Updegraff for their generous support, and the UCI Research Computing group especially Allen Schiano and Dana Roode.

References

Adams, L.: Mechanism for cb6r3_ae6_aq uses the following species, https://github.com/USEPA/CMAQ/blob/5.2/DOCS/User_Manual/Appendix_A/cb6r3_ae6_aq/CB6_species_table.md, 2017.

Amann, M., Klimont, Z., and Wagner, F.: Regional and global emissions of air pollutants: recent trends and future scenarios, Annual Review of Environment and Resources, 38, 31–55, 2013.

Aneja, V. P., Chauhan, J., and Walker, J.: Characterization of atmospheric ammonia emissions from swine waste storage and treatment lagoons, Journal of Geophysical Research: Atmospheres, 105, 11 535–11 545, 2000.

Appel, K. W., Bhave, P. V., Gilliland, A. B., Sarwar, G., and Roselle, S. J.: Evaluation of the community multiscale air quality (CMAQ) model version 4.5: sensitivities impacting model performance; part II—particulate matter, Atmospheric Environment, 42, 6057–6066, 2008.

Baek, B. H. and Aneja, V. P.: Measurement and analysis of the relationship between ammonia, acid gases, and fine particles in Eastern North Carolina, Journal of the Air & Waste Management Association, 54, 623–633, 2004.

Behera, S. N. and Sharma, M.: Investigating the potential role of ammonia in ion chemistry of fine particulate matter formation for an urban environment, Science of the Total Environment, 408, 3569–3575, 2010.

Behera, S. N., Sharma, M., Aneja, V. P., and Balasubramanian, R.: Ammonia in the atmosphere: a review on emission sources, atmospheric chemistry and deposition on terrestrial bodies, Environmental Science and Pollution Research, 20, 8092–8131, 2013.

Binkowski, F. S. and Roselle, S. J.: Models-3 Community Multiscale Air Quality (CMAQ) model aerosol component 1. Model description, Journal of geophysical research: Atmospheres, 108, 2003.

Boylan, J. W. and Russell, A. G.: PM and light extinction model performance metrics, goals, and criteria for three-dimensional air quality models, Atmospheric environment, 40, 4946–4959, 2006.

Byun, D. and Schere, K. L.: Review of the governing equations, computational algorithms, and other components of the Models-3 Community Multiscale Air Quality (CMAQ) modeling system, Applied mechanics reviews, 59, 51–77, 2006.

Eder, B. and Yu, S.: A performance evaluation of the 2004 release of Models-3 CMAQ, Atmospheric Environment, 40, 4811–4824, 2006.

EPA, U. S.: User's Guide to MOBILE6. 1 and MOBILE6. 2, Environmental Protection Agency, 2003.

EPA, U. S.: 2014 National Emissions Inventory (NEI) Technical Support Document (TSD), https://www.epa.gov/sites/production/files/2016-12/documents/nei2014v1_tsd.pdf, 2017a.

EPA, U. S.: SMOKE v4.5 User's Manual, https://www.cmascenter.org/smoke/documentation/4.5/manual_smokev45.pdf, 2017b.

Erisman, J. W., Sutton, M. A., Galloway, J., Klimont, Z., and Winiwarter, W.: How a century of ammonia synthesis changed the world, Nature Geoscience, 1, 636, 2008.

Friedl, M. A., Sulla-Menashe, D., Tan, B., Schneider, A., Ramankutty, N., Sibley, A., and Huang, X.: MODIS Collection 5 global land cover: Algorithm refinements and characterization of new datasets, Remote sensing of Environment, 114, 168–182, 2010.

Galloway, J. N., Townsend, A. R., Erisman, J. W., Bekunda, M., Cai, Z., Freney, J. R., Martinelli, L. A., Seitzinger, S. P., and Sutton, M. A.: Transformation of the nitrogen cycle: recent trends, questions, and potential solutions, Science, 320, 889–892, 2008.

Hong, S.-Y., Dudhia, J., and Chen, S.-H.: A revised approach to ice microphysical processes for the bulk parameterization of clouds and precipitation, Monthly Weather Review, 132, 103–120, 2004.

Hong, S.-Y., Noh, Y., and Dudhia, J.: A new vertical diffusion package with an explicit treatment of entrainment processes, Monthly weather review, 134, 2318–2341, 2006.

Horne, J. R., Zhu, S., Montoya, J., Hinks, M. L., Nizkorodov, S. A., and Dabdub, D.: Reactive Uptake of Ammonia by Secondary Organic Aerosols: Implications for Air Quality, Atmospheric Emvironment, Submitted, 2018.

Horowitz, L. W., Walters, S., Mauzerall, D. L., Emmons, L. K., Rasch, P. J., Granier, C., Tie, X., Lamarque, J.-F., Schultz, M. G., Tyndall, G. S., et al.: A global simulation of tropospheric ozone and related tracers: Description and evaluation of MOZART, version 2, Journal of Geophysical Research: Atmospheres, 108, 2003.

Jovan, S. and McCune, B.: Air-quality bioindication in the greater central valley of calfornia, with epophytic macrolichen communities, Ecological Applications, 15, 1712–1726, 2005.

Kain, J. S.: The Kain–Fritsch convective parameterization: an update, Journal of Applied Meteorology, 43, 170–181, 2004.

Krauter, C., Goorahoo, D., Potter, C., and Klooster, S.: Ammonia emissions and fertilizer applications in California's Central Valley, Emission Inventories-Partnering for the Future, 11, 15–18, 2002.

Laskin, A., Laskin, J., and Nizkorodov, S. A.: Chemistry of atmospheric brown carbon, Chemical reviews, 115, 4335–4382, 2015.

Laskin, J., Laskin, A., Nizkorodov, S. A., Roach, P., Eckert, P., Gilles, M. K., Wang, B., Lee, H. J., and Hu, Q.: Molecular selectivity of brown carbon chromophores, Environmental science & technology, 48, 12 047–12 055, 2014.

Lee, L., Wooldridge, P., Gilman, J., Warneke, C., De Gouw, J., and Cohen, R.: Low temperatures enhance organic nitrate formation: evidence from observations in the 2012 Uintah Basin Winter Ozone Study, Atmospheric Chemistry and Physics, 14, 12 441–12 454, 2014.

Lelieveld, J., Evans, J., Fnais, M., Giannadaki, D., and Pozzer, A.: The contribution of outdoor air pollution sources to premature mortality on a global scale, Nature, 525, 367–371, 2015.

Lin, Y.-H., Knipping, E., Edgerton, E., Shaw, S., and Surratt, J.: Investigating the influences of SO 2 and NH 3 levels on isoprene-derived secondary organic aerosol formation using conditional sampling approaches, Atmospheric Chemistry and Physics, 13, 8457–8470, 2013.

Liu, Y., Liggio, J., Staebler, R., and Li, S.-M.: Reactive uptake of ammonia to secondary organic aerosols: kinetics of organonitrogen formation, Atmospheric Chemistry and Physics, 15, 13 569–13 584, 2015.

Malm, W. C., Schichtel, B. A., Pitchford, M. L., Ashbaugh, L. L., and Eldred, R. A.: Spatial and monthly trends in speciated fine particle concentration in the United States, Journal of Geophysical Research: Atmospheres, 109, 2004.

McCulloch, R. B., Few, G. S., Murray, G. C., and Aneja, V. P.: Analysis of ammonia, ammonium aerosols and acid gases in the atmosphere at a commercial hog farm in eastern North Carolina, USA, Environmental Pollution, 102, 263–268, 1998.

Na, K., Song, C., Switzer, C., and Cocker, D. R.: Effect of ammonia on secondary organic aerosol formation from α-pinene ozonolysis in dry and humid conditions, Environmental science & technology, 41, 6096–6102, 2007.

NADP: Ambient Ammonia Monitoring Network (AMoN), http://nadp.sws.uiuc.edu/AMoN/AMoNFactSheet.pdf, 2014.

NCEP: National Weather Service, NOAA, U.S. Department of Commerce, NCEP FNL Operational Model Global Tropospheric Analyses, continuing from July 1999, https://doi.org/10.5065/D6M043C6, 2000.

Neuman, J., Nowak, J., Brock, C., Trainer, M., Fehsenfeld, F., Holloway, J., Hübler, G., Hudson, P., Murphy, D., Nicks, D., et al.: Variability in ammonium nitrate formation and nitric acid depletion with altitude and location over California, Journal of Geophysical Research: Atmospheres, 108, 2003.

Nowak, J., Neuman, J., Bahreini, R., Middlebrook, A., Holloway, J., McKeen, S., Parrish, D., Ryerson, T., and Trainer, M.: Ammonia sources in the California South Coast Air Basin and their impact on ammonium nitrate formation, Geophysical Research Letters, 39, 2012.

Otte, T. and Pleim, J.: The Meteorology-Chemistry Interface Processor (MCIP) for the CMAQ modeling system: updates through MCIPv3. 4.1, Geoscientific Model Development, 3, 243, 2010.

Park, R., Lee, S., Shin, S.-K., and Song, C. H.: Contribution of ammonium nitrate to aerosol optical depth and direct radiative forcing by aerosols over East Asia, Atmospheric Chemistry and Physics, 14, 2185–2201, 2014.

Pierce, T. E. and Waldruff, P. S.: PC-BEIS: a personal computer version of the biogenic emissions inventory system, Journal of the Air & Waste Management Association, 41, 937–941, 1991.

Pinder, R. W., Strader, R., Davidson, C. I., and Adams, P. J.: A temporally and spatially resolved ammonia emission inventory for dairy cows in the United States, Atmospheric Environment, 38, 3747–3756, 2004.

Pinder, R. W., Adams, P. J., Pandis, S. N., and Gilliland, A. B.: Temporally resolved ammonia emission inventories: Current estimates, evaluation tools, and measurement needs, Journal of Geophysical Research: Atmospheres, 111, 2006.

Pope III, C. A., Burnett, R. T., Thun, M. J., Calle, E. E., Krewski, D., Ito, K., and Thurston, G. D.: Lung cancer, cardiopulmonary mortality, and long-term exposure to fine particulate air pollution, Jama, 287, 1132–1141, 2002.

Pye, H.: CMAQv5.1 SOA Update, https://www.airqualitymodeling.org/index.php/CMAQv5.1_SOA_Update, 2016.

Pye, H. O., Pinder, R. W., Piletic, I. R., Xie, Y., Capps, S. L., Lin, Y.-H., Surratt, J. D., Zhang, Z., Gold, A., Luecken, D. J., et al.: Epoxide pathways improve model predictions of isoprene markers and reveal key role of acidity in aerosol formation, Environmental science & technology, 47, 11 056–11 064, 2013.

Russell, A. and Dennis, R.: NARSTO critical review of photochemical models and modeling, Atmospheric environment, 34, 2283–2324, 2000.

Seinfeld, J. H. and Pandis, S. N.: Atmospheric chemistry and physics: from air pollution to climate change, John Wiley & Sons, 2016.

Sheppard, L. J., Leith, I. D., Mizunuma, T., Neil Cape, J., Crossley, A., Leeson, S., Sutton, M. A., Dijk, N., and Fowler, D.: Dry deposition of ammonia gas drives species change faster than wet deposition of ammonium ions: evidence from a long-term field manipulation, Global Change Biology, 17, 3589–3607, 2011.

Skamarock, W., Klemp, J., Dudhia, J., Gill, D., Barker, D., Duda, M., Huang, X., Wang, W., and Powers, J.: A description of the Advanced Research WRF Version 3, NCAR technical note, Mesoscale and Microscale Meteorology Division, National Center for Atmospheric Research, Boulder, Colorado, USA, 2008.

Sutton, M., Pitcairn, C. E., and Fowler, D.: The exchange of ammonia between the atmosphere and plant communities, Advances in ecological research, 24, 301–393, 1993.

Updyke, K. M., Nguyen, T. B., and Nizkorodov, S. A.: Formation of brown carbon via reactions of ammonia with secondary organic aerosols from biogenic and anthropogenic precursors, Atmospheric environment, 63, 22–31, 2012.

USEPA: Guidance on the use of models and other analyses for demonstrating attainment of air quality goals for ozone, PM2. 5, and regional haze, US Environmental Protection Agency, Office of Air Quality Planning and Standards, 2007.

Vayenas, D. V., Takahama, S., Davidson, C. I., and Pandis, S. N.: Simulation of the thermodynamics and removal processes in the sulfate-ammonia-nitric acid system during winter: Implications for PM2. 5 control strategies, Journal of Geophysical Research: Atmospheres, 110, 2005.

Wang, Y., Zhang, Q., He, K., Zhang, Q., and Chai, L.: Sulfate-nitrate-ammonium aerosols over China: response to 2000–2015 emission changes of sulfur dioxide, nitrogen oxides, and ammonia, Atmospheric Chemistry and Physics, 13, 2635–2652, 2013.

Warner, J., Dickerson, R., Wei, Z., Strow, L., Wang, Y., and Liang, Q.: Increased atmospheric ammonia over the world's major agricultural areas detected from space, Geophysical Research Letters, 44, 2875–2884, 2017.

Weber, R. J., Guo, H., Russell, A. G., and Nenes, A.: High aerosol acidity despite declining atmospheric sulfate concentrations over the past 15 years, Nature Geoscience, 9, 282–285, 2016.

West, J. J., Ansari, A. S., and Pandis, S. N.: Marginal PM25: nonlinear aerosol mass response to sulfate reductions in the Eastern United States, Journal of the Air & Waste Management Association, 49, 1415–1424, 1999.

Xu, L. and Penner, J.: Global simulations of nitrate and ammonium aerosols and their radiative effects, Atmospheric Chemistry and Physics, 12, 9479–9504, 2012.

Yarwood, G., Jung, J., Whitten, G. Z., Heo, G., Mellberg, J., and Estes, M.: Updates to the Carbon Bond mechanism for version 6 (CB6), in: 2010 CMAS Conference, Chapel Hill, NC. October.(http://www. cmascenter. org/conference/2010/abstracts/emery_updates_carbon_2010. pdf), 2010.

Ye, X., Ma, Z., Zhang, J., Du, H., Chen, J., Chen, H., Yang, X., Gao, W., and Geng, F.: Important role of ammonia on haze formation in Shanghai, Environmental Research Letters, 6, 024 019, 2011.